18TH WORLD CONFERENCE ON EARTHQUAKE ENGINEERING
WCEE2024
MILAN

MILAN, ITALY
30TH JUNE - 5TH JULY 2024
www.wcee2024.it

Experimental study on the impact of an elastic spine in a structure with inerter-based devices

Sima Abolghasemi, Anika Sarkar, Carter Manson, Nicholas Wierschem[1] & Mark D. Denavit

Department of Civil and Environmental Engineering

Tickle College of Engineering, University of Tennessee, Knoxville, TN 37920, USA

[1]nwiersch@utk.edu

Abstract: *Vibration control devices can help protect structures from the effects of extreme loads, such as earthquakes. Inerters with relatively small physical mass can produce large mass effects through the conversion of translational motion to the rotational motion of a flywheel and have been proposed to be incorporated into a number of vibration control devices. Often inerter-based vibration control devices need to be distributed throughout a structure to be effective, as the concentration of these devices in a particular story of a typical structure would inhibit relative motion at that story without effectively controlling the global response of the structure. One strategy that has been considered to allow for the concentration of control devices in a structure is an elastic spine. An elastic spine is a stiff vertical structural element that runs the height of the building and is pinned at the building's base. While the elastic spine has demonstrated promise for enabling the concentration of other vibration control devices, its effectiveness has not been demonstrated with inerter-based control devices, which utilize a fundamentally different phenomenon. The goal of this study is to determine if the use of an elastic spine can allow for the effective concentration of inerter-based vibration control devices in a structure. For this investigation, a four-story model structure with and without an elastic spine is tested on a shake table using both recorded seismic and white noise ground motions. Configurations where inerters are installed at each story and configurations where multiple inerters are installed at a single story are examined. The impact of the combination of the elastic spine and the different inerter configurations is evaluated by examining the structure's dynamic properties and response to the ground motions. The results of this study show that, with an elastic spine, the system's seismic response and dynamic properties are insensitive to the inerter configuration. In contrast, without an elastic spine, the seismic response and system dynamic properties shift significantly depending on the inerter configuration. Given the results of this study, elastic spines show promise as a means of enabling efficient and effective designs where inerter-based vibration control devices are concentrated in a single story of a structure.*

1. Introduction

A recently proposed earthquake engineering strategy is coupling a primary structural system with a stiff elastic spine that runs the full height of the structure and is pinned at the base of the structure. The result of the addition of an elastic spine to a structural system, referred to subsequently in this work as a spine, is a nearly uniform drift profile along the height of the structure (Chen et al., 2018; Hu et al., 2021; Simpson and Mahin, 2018).

One of the key benefits of the nearly uniform drift profile that results from the spine is the prevention of soft story mechanisms that may lead to premature failure of the structure; thus, the inclusion of a spine often leads to a more ductile overall response in structures (Faramarzi and Taghikhany, 2021; Simpson and Mahin, 2018). The effectiveness of spines in structures has been studied numerically (Alavi and Krawinkler, 2004; Lai and Mahin, 2015; Qu et al., 2012) and experimentally (Abolghasemi et al., 2024; Chen and Tagawa, 2023; Ma et al., 2013). The effect of the spine's stiffness on its performance has been investigated (Chen et al., 2018; Lin et al., 2019), and design methodologies have been proposed (Chen et al., 2017; Simpson and Mahin, 2017).

The application of different types of energy dissipation devices and passive control devices in structures with spines has also been investigated. Hu et al. (2021) suggested the adoption of friction spring dampers with recentering capabilities that were distributed throughout the height of a steel structure featuring a pair of rigid spines. In a different approach, Qu et al. (2012) investigated the efficacy of shear-type steel dampers, which were distributed along the height of an eleven-story steel-reinforced concrete frame with pin-supported walls. Similarly, Wang et al. (2023) examined a pin-supported wall frame structure and explored the implementation of hysteretic and viscoelastic dampers within this framework. Furthermore, Palermo et al. (2021) numerically investigated a structure equipped with a spine, examining various configurations of viscous dampers within the system. These configurations included dampers positioned at every story, at selected stories, and concentrated at the base of the spine in a vertical configuration. The findings of this work showcased another key benefit of the elastic spine, as it indicated that the presence of the spine facilitated an enhancement in the seismic performance effectiveness across the different viscous damper configurations. Otherwise stated, the largely uniform story drifts resulting from the spine allow for more freedom in arranging (e.g., distributing throughout a structure vs. concentrating at one level) energy dissipation or passive control devices in structures. Abolghasemi et al. (2024) later conducted an experimental investigation on the impact of the arrangement of dampers in a structure with an elastic spine, referred to as a strongback, considering distributing throughout a structure vs. concentrating at one level. This experimental study had similar conclusions and found that the effective damping ratio, maximum story drift, and roof drift of the structure are significantly less sensitive to the location or arrangement of dampers in the presence of the strongback.

Inerters and inerter-based control devices have been considered as part of systems for mitigating the response of structures to earthquakes (Ma et al., 2021); however, these devices have not been studied for use in structures with spines. Inerters are two-terminal mechanical devices that produce resistive force proportional to the relative acceleration between their terminals. The proportionality constant of inerters has the same units as mass and is referred to as inertance. Physical mechanisms, including ball-screws and rack and pinion assemblies, can be used to realize inerters by converting translational motion into the rotational motion of a flywheel (Smith, 2012, 2002; Swift et al., 2013). This conversion allows inerters to produce large mass effects even though they may have a relatively small physical mass. For example, Sugimura et al. studied a device that has a flywheel with a physical mass of 560 kg that was capable of generating an effective mass of 5,400,000 kg (Sugimura et al., 2012). Due to its significant mass amplification capacity, inerters have been suggested for incorporation into a variety of vibration control systems (Di Egidio et al., 2021; Giaralis and Petrini, 2017; Hwang et al., 2007; Javidialesaadi and Wierschem, 2019; Nakamura et al., 2014).

While the effectiveness of different arrangements of energy dissipation and passive control devices in structures with spines has been investigated previously, the combination of inerters and a spine has not been previously considered. The inerter is fundamentally different than other structural control devices in that the intrinsic damping that is present in a realistic inerter is accompanied by large mass effects. Thus, the inerter's effect on a structure with a spine is unknown, as well as how various arrangements of inerters impacts the performance and behavior of the structure with and without a spine. For this investigation, a four-story primary structure with and without a spine was tested on a shake table using both recorded seismic and white noise ground motions. Configurations where inerters are installed at each story and configurations where multiple inerters are installed at a single story are examined. The impact of the combination of the spine and the different inerter configurations is evaluated by examining the structure's dynamic properties and response to the ground motions.

2. Physical model

A four-story model structure composed of a primary structure with an attached spine was used to conduct this experimental study. An isometric representation of the physical model is presented in Figure 1a. Important

details regarding this physical model are described in the following paragraphs; further details can be found in a document that includes this physical model's design drawings (Lifsey et al., 2023). This physical model was tested with different inerter configurations and with and without the spine attached to the primary structure.

This primary structure consists of five 457.2 mm x 457.2 mm x 12.7 mm aluminum floor plates, including the base and 16 spring steel columns with a width of 50.8 mm and thickness of 1.575 mm. The connections of the columns were made such that the bending span of the columns was equal to the clear story height, and the columns were orientated in the same direction so that the overall structure was flexible in one horizontal direction and ridge in the orthogonal horizontal direction. Each story measured 244.5 mm from center to center, while the height of the clear story was 231.8 mm.

The spine was constructed from two 76.2 mm x 1114.4 mm x 12.7 mm aluminum plates. The plates were joined together by several connector pieces. The spine was pinned at the base using a pair of partially threaded bolts. A combination of needle roller bearings and thrust bearings were utilized at the base pin to minimize the effect of friction in this pin. The base plate's centerline and the spine pin's centerline were at the same height. The orientation of the spine and the base pin was such that the spine rotated about this pin, given the motion of the structure in its flexible direction. Aluminum link arms measuring 38.1 mm in width and 12.7 mm in thickness, attached at the spine (left arm pin) and at brackets that were rigidly connected to the floor plates (right arm pin), were used to connect the spine to the primary structure at each floor. Needle roller bearings were used in the holes in the link arms at these pins to reduce friction. The centerline of the right arm pins was at the same elevation as the centerline of the floor plates.

Each floor weighed 8.083 kg when the related hardware (such as the bracket but not the link arm) was included. Each column weighed 0.154 kg. Each link arm weighed 0.576 kg. The spine weighed 10.156 kg when all the hardware was included. The spine's center of gravity was located 568.3 mm above the center of the spine's pin. The brackets attached to the floor plates remained in situations when the spine was not present, but the spine, link arms, and related hardware were removed.

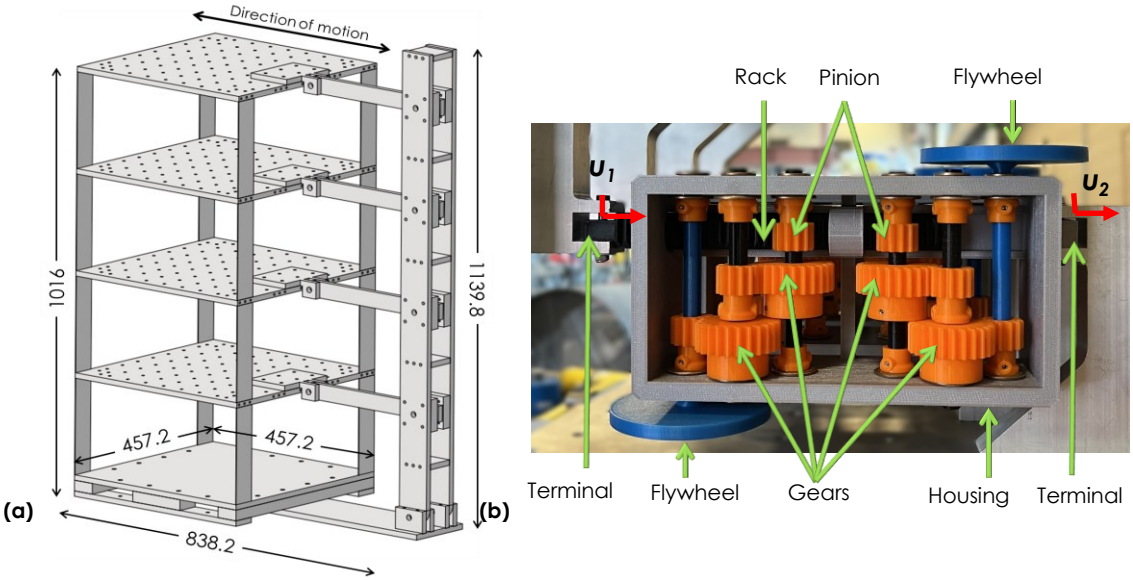

Figure 1: (a) Isometric view of the physical model of the primary structure with the spine – units are mm, (b) inerter used in this study with annotations identifying its components

The inerter in this study contains a pair of flywheels and a gearbox, which is comprised of a rack and pinion assembly and multiple gears in a housing (see Figure 1b). These inerters were fabricated predominantly via 3D printing with polylactic acid filament. The rack of the inerter, which is connected to one of the terminals of the device, slides within the inerter's housing along a linear path towards the other terminal, which is connected to the housing. The relative movement of the rack causes the pinion to rotate within the housing. The rotational velocity of the flywheels is further increased with a connected second set of gears. The rotational velocity of the flywheels and the relative velocity of the structure between the connection points of the inerter are related as follows:

$$\dot{\theta} = \alpha\left(\dot{u}_2 - \dot{u}_1\right) \tag{1}$$

where $\dot{\theta}$, $(\dot{u}_2 - \dot{u}_1)$, and α represent the rotational velocity of the flywheels, the relative velocity of the structure between the connection points of the inerter, and α is the coefficient governing this relationship, respectively. α for a rack and pinion mechanism with multiple gears is shown in Equation (2) where *n* is the number of gears; r_i and r_{pi} are the radius of the i[th] gear and its corresponding pinion, respectively; and r_f and r_{pf} are the flywheel radius, and radius of the flywheel pinion, respectively.

$$\alpha = \frac{{r_f}^2}{{r_{pf}}^2}\left(\prod_{i=1}^{n}\frac{r_i^2}{{r_{pi}}^2}\right) \tag{2}$$

The expression for the restoring force provided by an ideal inerter is

$$F = b\left(\ddot{u}_2 - \ddot{u}_1\right) \tag{3}$$

where the inerter is subjected to equal and opposite forces *F* at terminals 1 and 2 with accelerations $\ddot{u}_1$ and $\ddot{u}_2$. The coefficient on the relative acceleration term, *b,* in Equation (3) is known as the inertance and is equal to the effective mass provided by the ideal inerter. In addition to ideal inerter behavior, intrinsic friction in the rack and pinion mechanism will cause the relative motion of the inerter to result in energy dissipation.

Sets of aluminum brackets were utilized to connect the inerters within the stories of the primary structure; each bracket and associated connection hardware has a mass of 0.31 kg. The mass of a single inerter is 0.372 kg, with 0.06 kg of that mass associated with the flywheels and their attached axles. The inertance produced by the device was calculated to be 8.62 kg based on the geometry of the mechanism and the density of the materials utilized. The resulting mass amplification ratio as calculated by the inertance divided by the mass of the inerter is 22.0; alternatively, the mass amplification ratio as expressed as the inertance divided by the mass of only the flywheels and attached axles of the inerter is 141.

An additional second inerter configuration is considered that is identical to the configuration shown in Figure 1(b), except the device's axles with integrated flywheels have been replaced with axles without a flywheel. The result of this is an inerter that still has intrinsic friction but produces much less mass effects.

In this study, four inerters were attached in a variety of configurations to the primary structure: concentrated and distributed. When the inerters were concentrated in a single story, all four inerters were installed within a single story, following a symmetrical layout along the centerline of the floor. In contrast, when they were distributed, the four inerters were installed on the centerline of each story of the primary structure. In both arrangements, they aligned to engage in motion with the flexible direction of the structure. Photographs of the primary structure with the inerters concentrated in a single story and in the distributed arrangement are provided in Figure 2.

(a)  (b) 

Figure 2: (a) Primary structure with distributed inerter arrangement, (b) Primary structure with concentrated inerter arrangement

3. Description of experimental tests

This section provides an overview of the structural configurations, ground motions, and data collection procedures used in the experimental testing.

3.1. System configurations

Table 1 shows the system configurations employed in the experimental testing. These configurations include scenarios where all four inerters were concentrated in a single story, an arrangement with the inerters evenly distributed in each story, an arrangement with the inerters without flywheels evenly distributed in each story, and an arrangement where the inerters were removed from the primary structure. Each of these configurations was evaluated both with and without the spine, resulting in a total of fourteen distinct structural configurations for this investigation.

Table 1: System configurations for experimental tests

	Spine Config.	Config. Name	Number of Inerters at Each Story			
			1st	2nd	3rd	4th
Inerter Arrangement	Without	IC1	4	---	---	---
		IC2	---	4	---	---
		IC3	---	---	4	---
		IC4	---	---	---	4
		ID	1	1	1	1
		INFD	1	1	1	1
		NI	---	---	---	---
	With	IC1-S	4	---	---	---
		IC2-S	---	4	---	---
		IC3-S	---	---	4	---
		IC4-S	---	---	---	4
		ID-S	1	1	1	1
		INFD-S	1	1	1	1
		NI-S	---	---	---	---

The notation used to identify the configurations in Table 1 is also used when presenting the results of this study. IC1, IC2, IC3, and IC4 signify setups without the spine, where inerters are concentrated in the first, second, third, and fourth stories, respectively. ID refers to the distributed inerters configuration, where each story is equipped with one inerter, and this configuration is assessed in the absence of the spine. INFD refers to distributed inerters but with no flywheel utilized. NI is the configuration without an inerter attached. The same configurations, but with the inclusion of the spine, are indicated by appending "-S" to the respective configuration name.

3.2. Ground motions

Ground motions for these tests were generated using a six-degree-of-freedom shake table located at the University of Tennessee. A set of six distinct seismic ground motions (see Table 2) was employed to ensure a comprehensive evaluation and limit bias resulting from a single earthquake when assessing variations in the seismic response of the structural configurations.

The selected ground motions were recorded from historic seismic events and were sourced from the Pacific Earthquake Engineering Research (PEER) Center ground motion database (Ancheta et al., 2014). Only component A of the recorded ground motions was utilized. These ground motions were applied as unidirectional horizontal accelerations by the shake table; this direction of loading and motion is indicated in Figure 1. To ensure the physical model would not be damaged, thus enabling reuse for multiple tests, each of the selected ground motion records was individually scaled down. Detailed information regarding the properties of the six recorded seismic ground motions is presented in Table 2.

Table 2: Information on ground motions used for shake table tests

No.	Earthquake name	Station	Year	Mag.	Unscaled PGA max (g)	Scaled % used for the test
1	Northridge	Beverly Hills-Mulhol	1994	6.7	0.52	20
2	Kobe, Japan	Shin-Osaka	1995	6.9	0.24	50
3	Imperial Valley	El Centro Array #11	1979	6.5	0.38	40
4	Manjil, Iran	Abbar	1990	7.4	0.51	60
5	Chi-Chi, Taiwan	CHY101	1999	7.6	0.44	40
6	Landers	Coolwater	1992	7.3	0.42	50

The white noise ground motion record was scaled such that it induced a maximum structural response similar to that from the scaled seismic ground motion records. All seven ground motion records, including six seismic records and one shaped white noise, were applied in the flexible direction of the structure to each of the fourteen structure configurations listed in Table 1. This resulted in a total of 98 shake table tests, providing an assessment of seismic responses across different structural setups and loading scenarios.

3.3. Instrumentation and data acquisition

Accelerometers attached to the base and floors of the structure (Figure 3) were used to measure ground (shake table) accelerations and floor-level accelerations of the structure in its primary direction of motion. These measurements are used to estimate frequency response functions, as well as the structure's first mode frequency and damping ratio.

An NDI Optotrak optical measurement system was used to measure the position of each floor plate and the base plate by tracking the infrared light emitted from small markers attached to these components (Figure 3). These measurements were then used to calculate story drifts.

The system response to the white noise was used to estimate the structure's frequency response function, first mode frequency, and damping ratio for each system configuration. Numerical frequency response functions were estimated between the roof absolute acceleration and the base absolute acceleration using the tfestimate function in MATLAB (The MathWorks Inc, 2020a). Curve fitting was then used to match a single degree-of-freedom analytical dynamic model to the numerical frequency response functions produced from the experimental data using the system identification toolbox in MATLAB (The MathWorks Inc, 2020b).

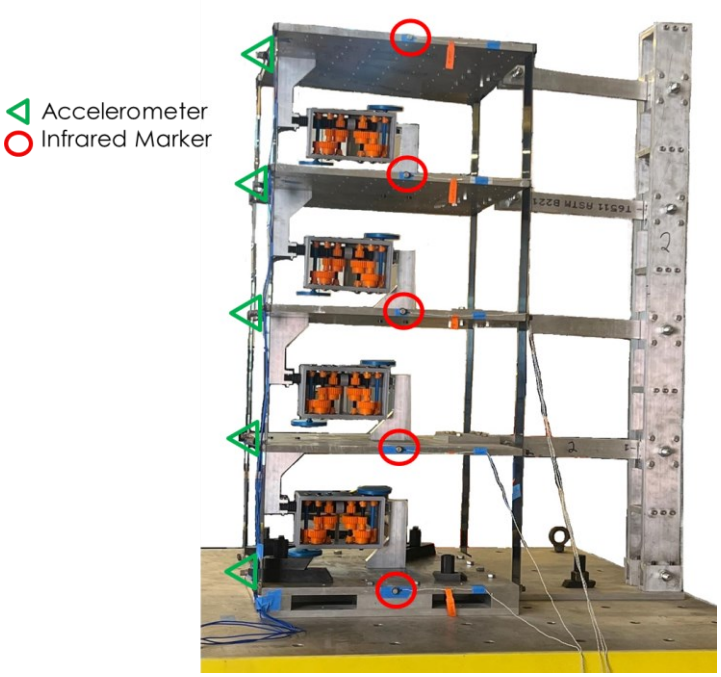

Figure 3. Physical model with instrumentation: accelerometers and infrared markers

4. Results and discussion

In this section, the results of the experimental shake table tests are presented and discussed. Frequency response functions (FRFs) are used to examine the dynamic behavior of the different inerter and spine system configurations. Additionally, maximum values from time history responses to the multiple ground motions are utilized to compare the performance of the different configurations.

Figure 4 shows the FRFs from the ground acceleration to the fourth-floor acceleration using data measured during the shaped white noise tests for each of the 14 configurations tested (Table 1). The different inerter configurations have different impacts on the dynamics of the system without the spine. Focusing on the first mode of the structure, which appears as a peak in each FRF near 1.8 Hz, without the spine, the different inerter configurations result in variations in the magnitude of the shift in this peak to lower frequencies and the reduction in the amplitude of this peak in comparison to the NI case. With the spine, the inerter configurations result in a relatively consistent shift in the first mode frequency and amplitude in comparison to the NI-S case. With and without the spine, the use of distributed inerters without a flywheel, INFD, and INDF-S, results in a shift of the first mode frequency and a reduction of the peak that is small in comparison to the changes seen with the use of distributed inerters with a flywheel, ID, and ID-S.

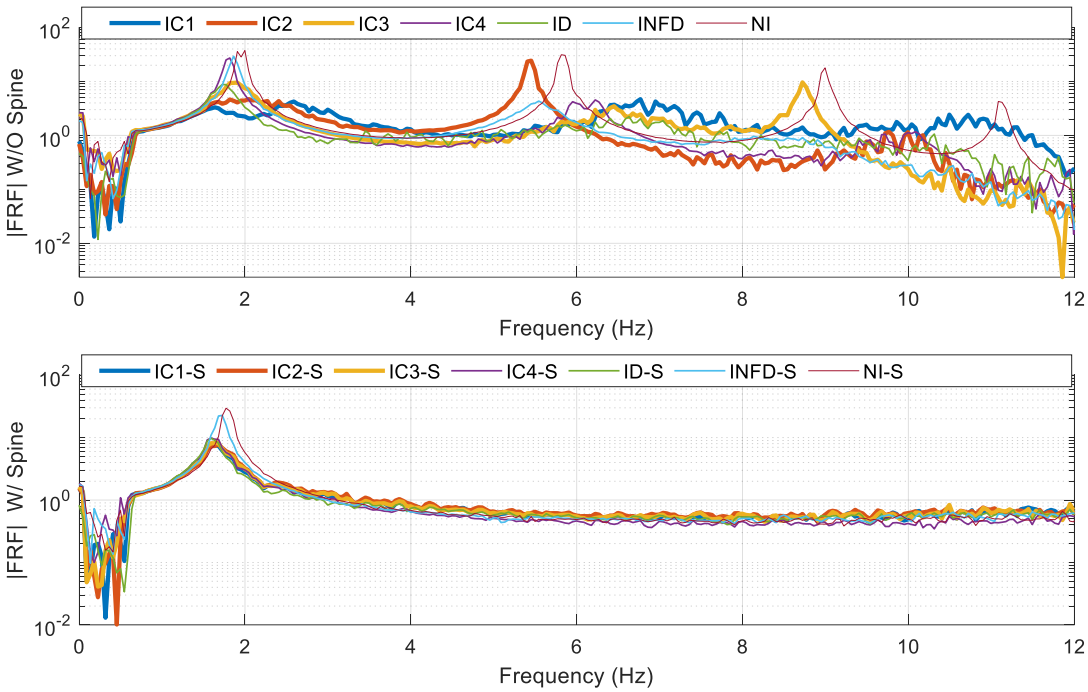

Figure 4: Frequency response functions from ground acceleration to fourth-floor acceleration for all system configurations

To provide a quantitative evaluation of the shifts in the first mode seen in Figure 4, Figure *5* shows the frequency of the first mode for each of the fourteen system configurations. The system frequencies seen in this figure were determined from fit models produced near the first mode of the FRFs from the ground acceleration to the fourth-floor acceleration using data obtained during the shaped white noise tests. For both with and without the spine, the lowest first mode frequencies are seen with the inerters concentrated in the first story or distributed throughout the structure. However, the results indicate a greater consistency in the first mode frequency with the spine for the configurations with inerters. The average of the first mode frequency of each set of configurations, excluding the no inerter and distributed inerters with no flywheel cases, are 1.88 Hz without the spine and 1.64 Hz with the spine. The standard deviation of these results is 0.25 Hz without the spine and 0.026 Hz with the spine.

Estimated damping values associated with the first mode frequency of each configuration were also determined from fit models produced near the first mode of the FRFs from the ground acceleration to the fourth-floor acceleration using data obtained during the shaped white noise tests and are shown in Figure 6.

The first mode damping ratio of the NI and NI-S configurations were 0.0165 and 0.0228, respectively. These results show the low intrinsic damping in the system, but that the structure with the spine has marginally higher damping, likely due to friction in the added pins. With the inerters without the flywheel distributed throughout the structure, the damping ratio increased to 0.0203 for the INFD case and 0.0277 for the INFD-S case. With the inerters (with a flywheel), the estimated damping without a spine significantly varies for the different inerter configurations. Some concentrated inerter configurations exhibit higher estimated damping than the distributed configuration (ID), and others have lower estimated damping values. In contrast, the estimated damping values with the spine show greater consistency for the different inerter configurations. The average first mode damping ratio of each set of configurations, excluding the no inerter and distributed inerters with no flywheel cases, are 0.089 without the spine and 0.064 with the spine. The standard deviation of these results is 0.090 without the spine and 0.028 with the spine.

The natural frequency and damping changes shown in Figure *5* and Figure 6 provide a good view of the overall system behavior shown in Figure 4 for the structures with a spine. The reason for this is that the drift pattern imposed by the spine suppresses the majority of the other global dynamics of the system. In contrast, the same is not true without the spine. As shown in Figure 4, without the spine, the different inerter configurations cause much more complicated changes in the systems. While larger effective damping is seen in most modes of the structure with the inerters and no spine, there are cases where modes with much less damping are seen, such as the mode near 5.5 Hz for IC2 and the mode near 8.5 Hz for IC3.

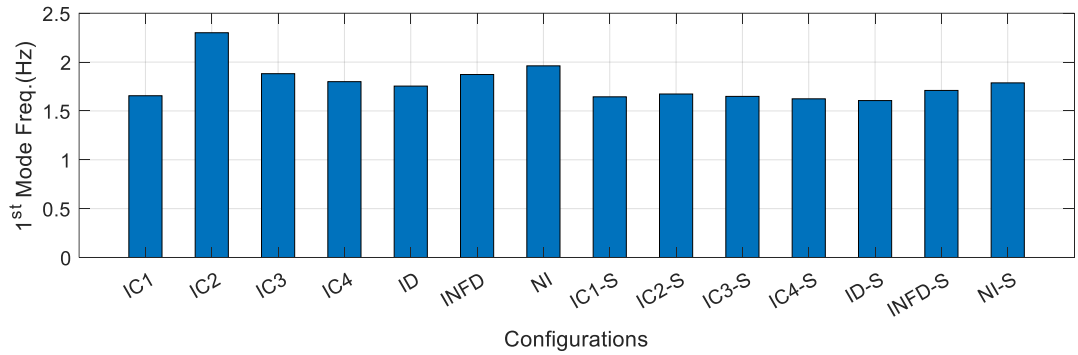

Figure 5: First mode frequency estimated by system identification for structure with and without spine and for all inerter configurations

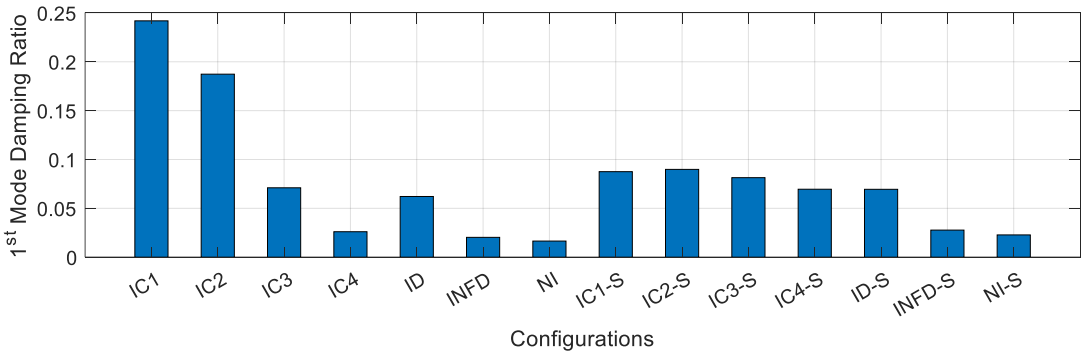

Figure 6: First mode damping ratio estimated by system identification for structure with and without spine and for all inerter configurations

Figure 7 shows the maximum story drift that results from the different system configurations for each of the seven ground motions considered. These results show that the inclusion of inerters significantly reduced the maximum story drift in the structure when compared to cases where no inerter was attached. This observation holds true with and without the spine. Furthermore, these results show that for the structure with a spine similar maximum story drift was observed with the different inerter configurations (IC1-S, IC2-S, IC3-S, IC4-S, and ID-S). In contrast, large variations in maximum story drift were observed for the inerter configurations without a spine (IC1, IC2, IC3, IC4, and ID).

Figure 7 also shows the maximum story drift results normalized with the results from the INFD configuration for systems without a spine and the results from the INFD-S configuration for systems with a spine. This normalization is done to account for changes in system response when the flywheels of the inerter produce significant mass effects. It is clear from these normalized results that with the spine, the performance of the inerters is consistent and almost always better than the no flywheel case. Without the spine, there are much larger variations in effectiveness based on inerter configuration and ground motion.

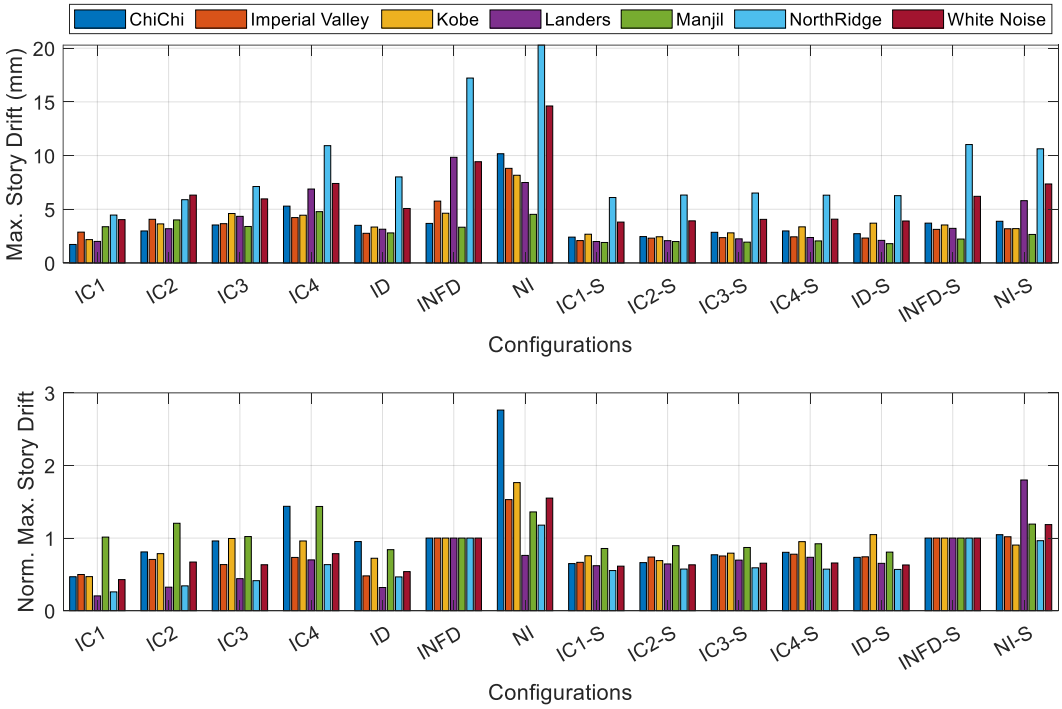

Figure 7: Maximum story drift and normalized maximum story drift results. Results were normalized with reference to the maximum story drift of the INFD configuration (for systems without a spine) and the INFD-S configuration (for systems with a spine)

Figure 8 presents the maximum absolute acceleration response for the different system configurations for the ground motions. When processing these time-history results, a lowpass filter with a cut off frequency of 100 Hz was used. The presence of a spine led to an increase in the maximum absolute acceleration compared to cases without a spine. Unlike the story drift results, there are no clear trends showing the presence or configuration of inerters improves the maximum acceleration performance of the structure.

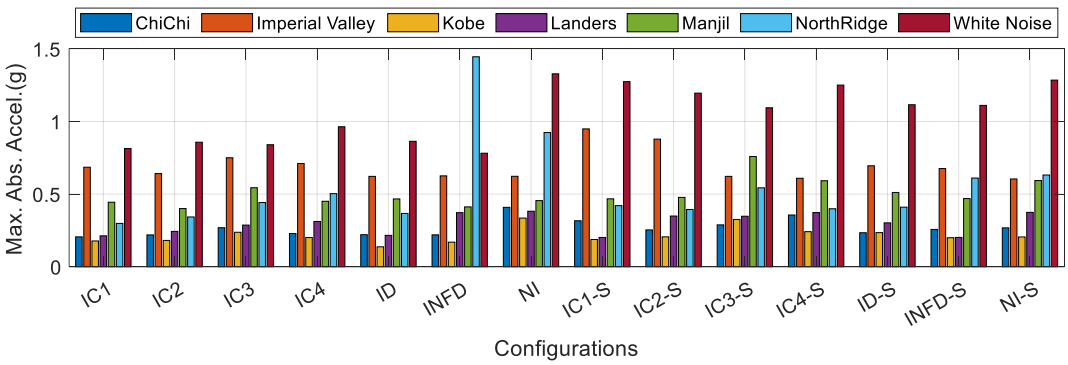

Figure 8: Maximum absolute acceleration results

Figure 9 shows plots of the maximum drifts for each story of the structure for each of the 14 configurations. This figure shows that the spine was able to impose a nearly uniform set of peak story drifts that is not seen in most cases for the structure without the spine. Furthermore, this figure shows how the magnitude of story drifts

changes for the different configurations of inerters (with flywheels) without the spine, but that these drifts remain more consistent with the spine.

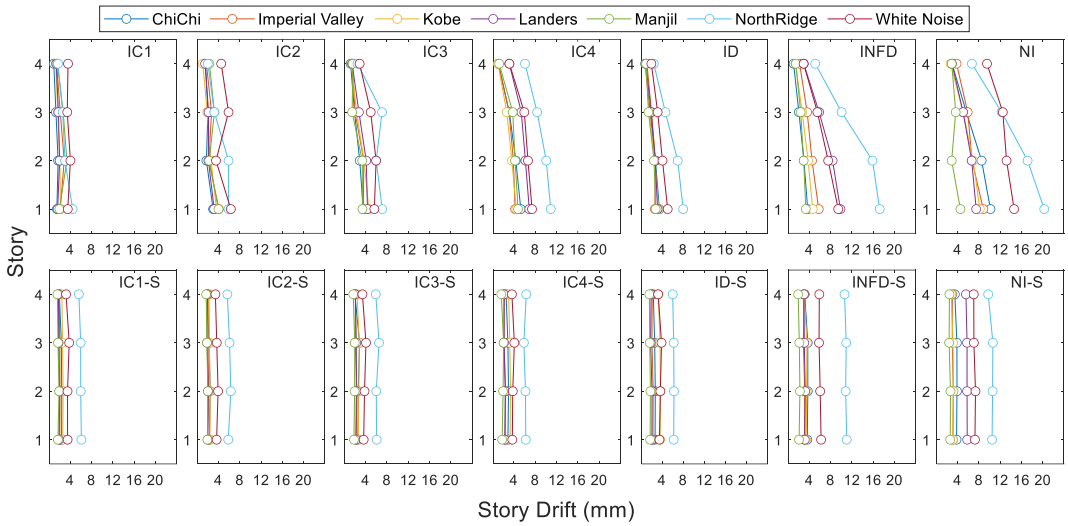

Figure 9: Maximum drifts for each story of the structure with and without spine for all inerter configurations

5. Conclusion

Inerters are a type of passive control device that can produce large effective mass by exploiting the conversion of translational motion to localized rotational motion. An experimental study was conducted on a small-scale four-story structure to investigate the behavior of a structure combining inerters and an elastic spine. Several configurations with inerters, including those where inerters are concentrated in a single floor and those where inerters are distributed across all floors, were tested with and without a spine using ground motions generated by a shake table. The key findings of this work are:

- The inclusion of inerters led to decreases in maximum story drift in most cases, but had no clear effect on maximum absolute acceleration.
- Inclusion of the spine led to a largely uniform distribution of story drift throughout the height of the structure, irrespective of the inerter configuration. In contrast, the story drift distribution varied widely for the inerter configurations without the spine.
- Without the spine, there was large variability in the effectiveness of the different inerter configurations and the impact of these configurations on the dynamic properties of the structure.
- With the spine and when the flywheels were attached, the different inerter configurations had largely similar effects on structural performance and dynamic properties.

The findings from this study indicate that when a spine is used, inerters can achieve comparable levels of effectiveness, whether they are distributed throughout a structure or concentrated in a single story. Further investigation into alternative inerter-based devices, especially tuned-inerter devices, is encouraged by these results. Tuned-inerter devices, which resemble tuned mass dampers in behavior, provide an effective and lightweight passive control option; however, they have not been utilized much in practice as they typically need to be distributed throughout a structure. This work shows that the addition of a spine may allow the concentration of tuned-inerter devices while still maintaining their effectiveness.

Acknowledgments

This research is based upon work supported by the National Science Foundation under Grant Nos. 1940197 and 1944513. Any opinions, findings, and conclusions or recommendations expressed in this material are those of the authors and do not necessarily reflect the views of the National Science Foundation.

References

Abolghasemi, S., Wierschem, N.E., Denavit, M.D., 2024. Impact of strongback on structure with varying damper and stiffness irregularity arrangements. Journal of Constructional Steel Research 213, 108333. https://doi.org/10.1016/j.jcsr.2023.108333

Alavi, B., Krawinkler, H., 2004. Strengthening of moment-resisting frame structures against near-fault ground motion effects. Earthquake Engineering & Structural Dynamics 33, 707–722. https://doi.org/10.1002/eqe.370

Ancheta, T.D., Darragh, R.B., Stewart, J.P., Seyhan, E., Silva, W.J., Chiou, B.S.-J., Wooddell, K.E., Graves, R.W., Kottke, A.R., Boore, D.M., Kishida, T., Donahue, J.L., 2014. NGA-West2 Database. Earthquake Spectra 30, 989–1005. https://doi.org/10.1193/070913EQS197M

Chen, C.H., Tsai, I.J., Tang, Y., 2017. Drift Concentration of a Three-Story Special Concentrically Braced Frame with Strongback under Earthquake Loading. AMM 863, 287–292. https://doi.org/10.4028/www.scientific.net/AMM.863.287

Chen, X., Tagawa, H., 2023. Seismic performance of rocking-delayed spine frame system with base initial gaps. Earthquake Engineering and Resilience 2, 131–157. https://doi.org/10.1002/eer2.39

Chen, X., Takeuchi, T., Matsui, R., 2018. Seismic Performance and Evaluation of Controlled Spine Frames Applied in High-rise Buildings. Earthquake Spectra 34, 1431–1458. https://doi.org/10.1193/080817EQS157M

Di Egidio, A., Pagliaro, S., Fabrizio, C., 2021. Combined Use of Rocking Walls and Inerters to Improve the Seismic Response of Frame Structures. J. Eng. Mech. 147, 04021016. https://doi.org/10.1061/(ASCE)EM.1943-7889.0001920

Faramarzi, M.S., Taghikhany, T., 2021. A comparative performance-based seismic assessment of strongback steel braced frames. Journal of Building Engineering 44, 102983. https://doi.org/10.1016/j.jobe.2021.102983

Giaralis, A., Petrini, F., 2017. Wind-Induced Vibration Mitigation in Tall Buildings Using the Tuned Mass-Damper-Inerter. J. Struct. Eng. 143, 04017127. https://doi.org/10.1061/(ASCE)ST.1943-541X.0001863

Hu, S., Wang, W., Qu, B., 2021. Self-centering companion spines with friction spring dampers: Validation test and direct displacement-based design. Engineering Structures 238, 112191. https://doi.org/10.1016/j.engstruct.2021.112191

Hwang, J.-S., Kim, J., Kim, Y.-M., 2007. Rotational inertia dampers with toggle bracing for vibration control of a building structure. Engineering Structures 29, 1201–1208. https://doi.org/10.1016/j.engstruct.2006.08.005

Javidialesaadi, A., Wierschem, N.E., 2019. Energy transfer and passive control of single-degree-of-freedom structures using a one-directional rotational inertia viscous damper. Engineering Structures 196, 109339. https://doi.org/10.1016/j.engstruct.2019.109339

Lai, J.-W., Mahin, S.A., 2015. Strongback System: A Way to Reduce Damage Concentration in Steel-Braced Frames. Journal of Structural Engineering 141, 04014223. https://doi.org/10.1061/(ASCE)ST.1943-541X.0001198

Lifsey, P., Drake, C., Wierschem, N., Abolghasemi, S., Denavit, M., 2023. Structural Design Drawings. https://doi.org/10.17603/ds2-r5wm-6b46

Lin, J.-L., Kek, M.-K., Tsai, K.-C., 2019. Stiffness configuration of strongbacks to mitigate inter-story drift concentration in buildings. Engineering Structures 199, 109615. https://doi.org/10.1016/j.engstruct.2019.109615

Ma, R., Bi, K., Hao, H., 2021. Inerter-based structural vibration control: A state-of-the-art review. Engineering Structures 243, 112655. https://doi.org/10.1016/j.engstruct.2021.112655

Ma, X., Krawinkler, H., Deierlein, G.G., 2013. Seismic Design and Behavior of Self-Centering Braced Frame with Controlled Rocking and Energy Dissipating Fuses, John A. Blume Earthquake Engineering Center, Technical Report 174.

Nakamura, Y., Fukukita, A., Tamura, K., Yamazaki, I., Matsuoka, T., Hiramoto, K., Sunakoda, K., 2014. Seismic response control using electromagnetic inertial mass dampers: Seismic response control using EIMD. Earthquake Engng Struct. Dyn. 43, 507–527. https://doi.org/10.1002/eqe.2355

Palermo, M., Laghi, V., Gasparini, G., Silvestri, S., Trombetti, T., 2021. Seismic Design and Performances of Frame Structures Connected to a Strongback System and Equipped with Different Configurations of Supplemental Viscous Dampers. Frontiers in Built Environment 7.

Qu, Z., Wada, A., Motoyui, S., Sakata, H., Kishiki, S., 2012. Pin-supported walls for enhancing the seismic performance of building structures. Earthquake Engineering & Structural Dynamics 41, 2075–2091. https://doi.org/10.1002/eqe.2175

Simpson, B., Mahin, S., 2017. ANALYTICAL INVESTIGATION OF OFFSET GEOMETRIES IN STEEL STRONGBACK BRACED FRAMES, in: Eleventh U.S. National Conference on Earthquake

Engineering. Presented at the Eleventh U.S. National Conference on Earthquake Engineering, Los Angeles, California, June 25-29, 2018.
Simpson, B.G., Mahin, S.A., 2018. Experimental and Numerical Investigation of Strongback Braced Frame System to Mitigate Weak Story Behavior. Journal of Structural Engineering 144, 04017211. https://doi.org/10.1061/(ASCE)ST.1943-541X.0001960
Smith, M.C., 2012. Force-Controlling Hydraulic Device. US 2021/0199428 A1.
Smith, M.C., 2002. Synthesis of mechanical networks: the inerter. IEEE Trans. Automat. Contr. 47, 1648–1662. https://doi.org/10.1109/TAC.2002.803532
Sugimura, Y., Goto, W., Saito, K., Nimomiya, T., Tanizawa, H., 2012. Sugimura, Y., Goto, W., Tanizawa, H., Saito, K. and Nimomiya, T., 2012, September. Response control effect of steel building structure using tuned viscous mass damper. In Proceedings of the 15th world conference on earthquake engineering (Vol. 9, pp. 24-28). pp. 24–28.
Swift, S.J., Smith, M.C., Glover, A.R., Papageorgiou, C., Gartner, B., Houghton, N.E., 2013. Design and modelling of a fluid inerter. International Journal of Control 86, 2035–2051. https://doi.org/10.1080/00207179.2013.842263
The MathWorks Inc, 2020a. MATLAB version: 9.9 (R2020b).
The MathWorks Inc, 2020b. System Identification Toolbox version: 9.13 (R2020b).
Wang, X., Qu, Z., Gong, T., 2023. Role of dampers on the seismic performance of pin-supported wall-frame structures. Earthq. Eng. Eng. Vib. 22, 453–467. https://doi.org/10.1007/s11803-022-2092-5